

# Simultaneous Compression and Quantization: A Joint Approach for Efficient Unsupervised Hashing

Tuan Hoang\* Thanh-Toan Do<sup>+</sup> Dang-Khoa Le-Tan\* Ngai-Man Cheung\*

\* Singapore University of Technology and Design (SUTD)

nguyenanhtuan.hoang@mymail.sutd.edu.sg, {letandang.khoa, ngaiman.cheung}@sutd.edu.sg

<sup>+</sup> The University of Adelaide

thanh-toan.do@adelaide.edu.au

## Abstract

*The two most important requirements for unsupervised data-dependent hashing methods are to preserve similarity in the low-dimensional feature space and to minimize the binary quantization loss. Even though there are many hashing methods that have been proposed in the literature, there is room for improvement to address both requirements simultaneously and adequately.*

*In this paper, we propose a novel approach, named **Simultaneous Compression and Quantization (SCQ)**, to jointly learn to compress and binarize input data in a single formulation. A simple scale pre-processing is introduced to help to preserve data similarity. With this approach, we introduce a loss function and its relaxed version, termed *Orthonormal Encoder (OnE)* and *Orthogonal Encoder (OgE)* respectively, which involve the challenging binary and orthogonal constraints. We then propose novel algorithms that can effectively handle these challenging constraints. Comprehensive experiments on unsupervised image retrieval show that our proposed methods consistently outperform other state-of-the-art hashing methods while still being very computationally-efficient.*

## 1. Introduction

For decades, image hashing has been an active research field in the vision community [1, 10, 32, 35]. Under specific conditions [10], image hashing has great advantages in storage and computation speed for similarity search/retrieval, especially in the application of Content-based Image Retrieval [7, 3, 14]. Firstly, the binary code should be short so as to the whole hash table can fit in the memory. Secondly, the binary code should preserve the similarity, i.e., (dis)similar images have (dis)similar hashing codes in the Hamming distance space. Finally, the algorithm to learn parameters should be fast and for unseen samples, the hashing method should produce the hash codes efficiently. It is

very challenging to simultaneously satisfy all three requirements, especially, under the binary constraint which leads to an NP-hard mixed-integer optimization problem.

The proposed hashing methods in literature can be categorized into data-independence [9, 17, 22] and data-dependence; in which, the latter recently receives more attention in both (semi-)supervised [16, 18, 19, 20, 25] and unsupervised [2, 4, 5, 10, 12, 13] manners. However, in practice, labeled datasets are limited and costly; hence, in this work, we focus only on the unsupervised setting. We refer readers to recent surveys [11, 29, 30, 31] for more detailed reviews of data-independent/dependent hashing methods.

### 1.1. Related works

The most relevant work to our proposal is Iterative Quantization (ITQ) [10], which is a very fast and competitive hashing method. The fundamental of ITQ is two folds. Firstly, to achieve low-dimensional features, it uses the well-known Principle Component Analysis (PCA) method. PCA maximizes the variance of projected data and keeps dimensions pairwise uncorrelated. Hence, the low-dimension data, projected using the top PCA component vectors, can preserve data similarity well. Secondly, minimizing the binary quantization loss using an orthogonal rotation matrix strictly maintains the data pairwise distance. As a result, ITQ learns binary codes that can highly preserve the local structure of the data. However, optimizing these two steps separately, especially when no binary constraint is considered in the first step, i.e., PCA, leads to suboptimal solutions. In contrast, our proposed formulation optimizes the projection variation and the quantization loss simultaneously.

Other works relevant to our proposed method are Binary Autoencoder (BA) [2], Relaxed Binary Autoencoder (RBA) [6] and UH-BDNN [4]. In these methods, the authors proposed to combine the data dimension reduction and binary quantization into a single step by using encoder

of autoencoder, while the decoder encourages (dis)similar inputs map to (dis)similar binary codes. However, the reconstruction criterion is not a direct way for preserving the similarity [4]. Additionally, even achieving very competitive performances, UH-BDNN is based on the deep neural network (DNN); hence, it is difficult to produce the binary code computationally-efficiently.

## 1.2. Contribution

In this work, to address the problem of learning to preserve data affinity in low-dimension binary codes, we first propose a novel loss function to learn a single linear transformation under the *column semi-orthonormal constraint*<sup>1</sup> in the unsupervised manner that *compresses and binarizes the input data jointly*. While this linear transformation generally does not guarantee to retain high variance components of the dataset, we secondly show that by applying an appropriate *scale pre-processing*, this linear transformation can be learned to retain high variance components, i.e., well preserve the local structure of data. We then propose to relax the *column semi-orthonormal* constraint to *column semi-orthogonal* constraint that not only helps to gain extra retrieval performances but also significantly improves the training time.

Our proposed loss functions are confronted with two main challenges including the binary constraint, which is the traditional and well-known difficulty of hashing problem [1, 10, 32], and the orthonormal/orthogonal constraint, which is non-convex [33]. To tackle the binary constraint, we propose to apply an alternating optimization with an auxiliary variable and resolve the orthonormal/orthogonal constraint by using the discrete coordinate descent approach to learn one column of the projection matrix at a time while fixing the others. The proposed methods are named as Orthonormal Encoder (OnE) and Orthogonal Encoder (OgE).

Comprehensive experiments on common benchmark datasets show considerable improvements on retrieval performance of proposed methods over other state-of-the-art hashing methods. Additionally, the training time and online processing time are also discussed to show the computational efficiency of our methods.

## 1.3. Notations and Term definitions

We first introduce the notations. Given a zero-centered dataset  $\mathbf{X} = \{\mathbf{x}_i\}_{i=1}^n \in \mathbb{R}^{n \times d}$  which consists of  $n$  images and each image is represented by a  $d$ -dimension feature descriptor, our proposed hashing methods aim to learn a column semi-orthonormal/semi-orthogonal matrix  $\mathbf{V} \in \mathbb{R}^{d \times L}$  ( $L \ll d$ ) which simultaneously compresses input data  $\mathbf{X}$  to  $L$ -dimensional space, while retains a high amount of variation, and quantizes to binary codes  $\mathbf{B} \in \{-1, +1\}^{n \times L}$ .

<sup>1</sup>Please refer to Section 1.3 for our term definitions.

It is important to note that, in this work, we abuse the terms: *column semi-orthonormal/semi-orthogonal matrix*. Specifically, the term *column semi-orthonormal matrix* is used to indicate the matrix  $\mathbf{V}$  that  $\mathbf{V}^T \mathbf{V} = \mathbf{I}_{L \times L}$ , where  $\mathbf{I}_{L \times L}$  is the  $L \times L$  identity matrix. While the term *column semi-orthogonal matrix* indicates matrix  $\mathbf{V}$  that  $\mathbf{V}^T \mathbf{V} = \mathbf{D}_{L \times L}$ , where  $\mathbf{D}_{L \times L}$  is an arbitrary  $L \times L$  diagonal matrix. The word “semi” is prepended to “orthonormal/orthogonal” to indicate that the matrix is non-square and the word “column” means that columns of the matrix are pairwise independent.

We define  $\hat{\Lambda} = [\lambda_d, \dots, \lambda_1]$  as the eigenvalues of the covariance matrix  $\mathbf{X}^T \mathbf{X}$  sorted in ascending order. Finally, let  $\mathbf{b}_k, \mathbf{v}_k$  be the  $k$ -th ( $1 \leq k \leq L$ ) columns of  $\mathbf{B}, \mathbf{V}$  respectively.

## 2. Simultaneous Compression & Quantization: Orthonormal Encoder

### 2.1. Problem Formulation

In order to jointly learn data dimension reduction and binary quantization using a single linear transformation  $\mathbf{V}$ , we propose to solve the following constrained optimization:

$$\begin{aligned} \arg \min_{\mathbf{B}, \mathbf{V}} \mathcal{Q}(\mathbf{B}, \mathbf{V}) &= \frac{1}{n} \|\mathbf{B} - \mathbf{XV}\|_F^2 \\ \text{s.t. } \mathbf{V}^T \mathbf{V} &= \mathbf{I}_{L \times L}; \mathbf{B} \in \{-1, +1\}^{n \times L}, \end{aligned} \quad (1)$$

where  $\|\cdot\|_F$  denotes the Frobenius norm. Note that  $\mathbf{V}$  is constrained to be a column semi-orthonormal matrix, which is necessary to make sure no redundant information is captured in binary codes [28] and the projection vectors do not scale up/down projected data.

It is noteworthy that even though the loss function Eq. (1) is similar to the binary quantization loss function of ITQ [10], their fundamentals are different. Firstly, our approach works directly on the original high-dimensional feature space  $\mathbf{X}$ , instead of on the compressed low-dimensional feature space after using PCA. This leads to the second main difference that the column semi-orthonormal matrix  $\mathbf{V}$  simultaneously (i) *compresses data* to low-dimension with high amount of retained variation; in section 2.2, we provide detailed analysis on how Eq. (1) can accomplish this non-trivial task; and (ii) *quantizes to binary codes* instead of just minimizing the quantization loss by using an orthogonal matrix as in ITQ. Finally, the optimization Eq. (1) is challenging since there is no easy way for solving for non-square  $\mathbf{V}$ . In section 2.3, we propose a novel and efficient algorithm to handle this difficulty.

### 2.2. Balancing retained variation and quantization loss

In the loss function Eq. (1), we do not explicitly maximize the retained variation of projected data, which is

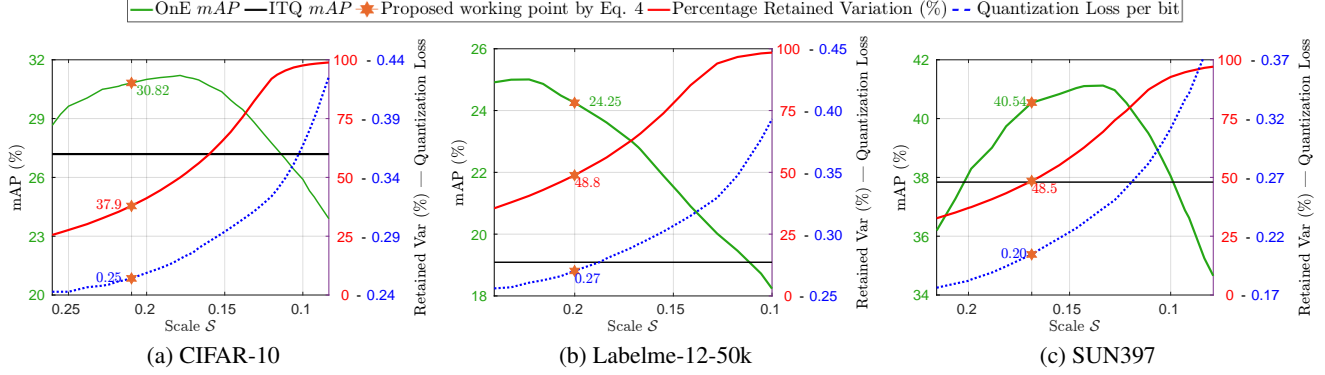


Figure 1: Analyzing the effects of the scale value  $\mathcal{S}$  on (i) the quantization loss per bit (blue dash line with blue right Y-axis), (ii) the percentage of total retained variation by the minimizing quantization loss projection matrix in comparison with the total retained variation of top- $L$  PCA components (red line with red right Y-axis), and (iii) the retrieval performance (green line with green left Y-axis). The baseline retrieval performance of ITQ [10] is included for easier comparison (black line with green left Y-axis). To obtain each data point, we solve the problem Eq. (1) at various scale values  $\mathcal{S}$ , i.e., replace  $\mathcal{S}\mathbf{X}$  with  $\mathbf{X}$  in Eq. (1), and use Algorithm 1 (section 2.3) to tackle the optimization. We use VGG-FC7 feature descriptors of CIFAR-10, Labelme-12-50k, and SUN397 datasets<sup>2</sup> at  $L = 32$ . Note that x-axis is in descending order.

an important condition to preserve local structure of data. Hence, before discussing how to solve the problem, in this section, we show that by applying an appropriate scale  $\mathcal{S}$  on the dataset we can control the amount of retained variation and achieve small quantization loss in the minimizing quantization loss problem. Noticeably, by applying any positive scale  $\mathcal{S} > 0$ <sup>3</sup> on the dataset, the local structure of data is strictly preserved, i.e., the ranking nearest neighbor set of every data point is always the same. Therefore, in the hashing problem for retrieval task, it is equivalent to work on a scaled version of the dataset, i.e.,  $\mathbf{X}_{\mathcal{S}} = \mathcal{S}\mathbf{X}$ . Thus, the loss function of Eq. (1) can be re-written as following:

$$\mathcal{Q}(\mathcal{S}, \mathbf{V}) = \|\mathbf{1} - \mathcal{S}|\mathbf{X}\mathbf{V}|\|_F^2 \quad \text{s.t. } \mathbf{V}^T \mathbf{V} = \mathbf{I}_{L \times L}; \mathcal{S} > 0, \quad (2)$$

where  $|\cdot|$  is the operation to find the absolute values and  $\mathbf{1}$  is the all-1 ( $n \times L$ ) matrix.

Considering the Fig. 1 which shows the analysis of the effects of the scale value  $\mathcal{S}$  on (i) the quantization loss per bit, (ii) the total retained variation by the minimizing quantization loss projection matrix in comparison with the total retained variation of top- $L$  PCA components, and (iii) the retrieval performance<sup>4</sup>, we cannot achieve a scale value  $\mathcal{S}$  that can simultaneously maximizes the retained variation and minimizes the optimal quantization loss. On the one hand, as the scale value  $\mathcal{S}$  decreases, minimizing the loss function Eq. (2) produces a projection matrix that focuses on high-variance directions, i.e., retains more variation in comparison with PCA (red line). On the other hand, at smaller  $\mathcal{S}$ , the quantization loss is much larger (blue dash

line). We will discuss how to automatically determine an appropriate  $\mathcal{S}$  that can achieve good trade-off between retained variation and quantization loss.

### 2.2.1 Maximizing retained variation

We recognize that by scaling to the dataset  $\mathbf{X}$  by a small scale value  $\mathcal{S}$ , such that all projected data points are inside the hyper-cube of 1, i.e.,  $\max(\mathcal{S}|\mathbf{X}\mathbf{V}|) \leq 1$ , the *minimizing quantization loss problem* can achieve similar results to the *maximizing retained variation problem*, i.e.,  $\arg \max_{\mathbf{V}} \|\mathcal{S}\mathbf{X}\mathbf{V}\|_F^2 \approx \arg \min_{\mathbf{V}} \|\mathbf{1} - \mathcal{S}|\mathbf{X}\mathbf{V}|\|_F^2$ , in which  $\mathbf{V}^T \mathbf{V} = \mathbf{I}_{L \times L}$ . Intuitively, we can interpret the PCA problem as to find the projection that maximizes the distances of projected data points from the coordinate origin, while the minimizing quantization loss problem tries to find the projection matrix that minimizes the distances of projected data points from  $-1$  or  $+1$  correspondingly. Since each vector of  $\mathbf{V}$  is constrained to have the unit norm, the condition  $\max(\mathcal{S}|\mathbf{X}\mathbf{V}|) \leq 1$  actually can be satisfied by scaling the dataset by  $\mathcal{S}_{\max\_var}$ , where  $1/\mathcal{S}_{\max\_var}$  is equal to the largest  $l_2$ -distance between data points and the coordinate origin, to have all data points in the original space inside the hyper-ball with unit radius. The experimental results in Fig. 1 are strongly support this claim. Specifically, as  $\mathcal{S}$  gets smaller (and approaches  $\mathcal{S}_{\max\_var}$ , which approximate 0.01 for the datasets in Fig. 1), minimizing quantization loss projection matrix can help to retain more variation (and up to over 99% of variation) in comparison with PCA.

### 2.2.2 Minimizing quantization loss

Regarding the quantization loss  $\mathcal{Q}(\mathcal{S}, \mathbf{V})$  (Eq. 2), which is a convex function of  $\mathcal{S}|\mathbf{X}\mathbf{V}|$ , by setting

<sup>2</sup>Please refer to Section 4.1 for more details about the datasets and performance evaluation.

<sup>3</sup>For simplicity, we only discuss positive scale value  $\mathcal{S} > 0$ . Negative scale value  $\mathcal{S} < 0$  should have similar effects.

<sup>4</sup>Please refer to image caption for more detail.

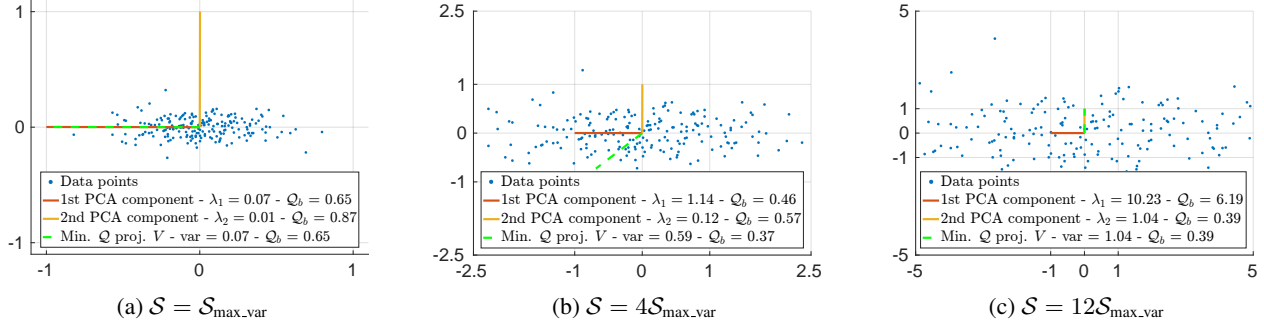


Figure 2: A toy example for  $n = 200$ ,  $d = 2$  and  $L = 1$  to illustrate how the quantization loss and the minimizing quantization loss vector (green dash line) vary when  $S$  increases. The values in legends represent the variances and the quantization losses per bit,  $Q_b$ , of the data which is projected in corresponding vectors (rounding to two decimal places).

$\partial Q(S, \mathbf{V}) / \partial S |\mathbf{XV}| = \mathbf{0}$ , we have the optimal solution for  $Q(S, \mathbf{V})$  as following:

$$\frac{\partial Q(S, \mathbf{V})}{\partial S |\mathbf{XV}|} = 2(S |\mathbf{XV}| - \mathbf{1}) = \mathbf{0} \Leftrightarrow \begin{cases} \text{mean}(|\mathbf{XV}|) = 1/S \\ \text{var}(|\mathbf{XV}|) = 0 \end{cases} \quad (3)$$

where  $\mathbf{0}$  is the all-0 ( $n \times L$ ) matrix.

Considering  $S \geq S_{\max\_var}$ , there are two important findings. Firstly, there is obviously no scaling value  $S$  that can concurrently achieve  $S \max(|\mathbf{XV}|) \leq 1$  and  $S \text{mean}(|\mathbf{XV}|) = 1$ , except the case  $S |\mathbf{XV}| = \mathbf{1}$  which is unreal in practice. Secondly, from Eq. (3), we also can recognize that as  $S$  gets larger, i.e.,  $1/S$  gets smaller, minimizing the loss  $Q$  will produce  $\mathbf{V}$  that focuses on lower-variance directions so as to achieve smaller  $\text{mean}(|\mathbf{XV}|)$  as well as smaller  $\text{var}(|\mathbf{XV}|)$ , i.e.,  $S |\mathbf{XV}|$  gets closer to the global minimum of  $Q(S, \mathbf{V})$ . Consequently, the quantization loss becomes smaller. This explanation is consistent with the observation in Fig. 1 that the quantization loss and the retained variation simultaneously reduce when  $S$  increases. However, keeping increasing  $S$  when  $\mathbf{V}$  already focuses on least-variance directions will make the quantization loss larger.

In Fig. 2, we show a toy example to illustrate that as  $S$  increases, the minimizing quantization loss projection vector diverts from top-PCA component (Fig. 2a) to smaller variance directions (Fig. 2b  $\rightarrow$  2c), while the quantization loss (per bit) gets smaller (Fig. 2a  $\rightarrow$  2c).

### 2.2.3 Quantization loss Vs. Retained variation

Since both quantization loss and retained variation are critical in the hashing problem, it is necessary to make a trade-off between these two requirements. So, “How to determine the scalar value that can properly scale the dataset?” As data variation varies from dataset to dataset, it is difficult to find the optimal scale value for all datasets (Fig. 1: green line). Therefore, the scale value should be determined from the dataset itself. In particular, we leverage the

eigenvalues, which are the variances of PCA components, to find the scaling value. Specifically, we empirically found that dividing the dataset by the square root of the  $(L/2)$ -th eigenvalue, i.e.,

$$S^* = 1 / \sqrt{\lambda_{(L/2)}} \quad (4)$$

generally achieves a good trade-off between quantization loss and retained variation. In fact, as shown in Fig. 1, our proposed method works well and outperforms ITQ [10] for a wide range of scale values (black line). It is worth noting that ITQ [10] does not care about scaling.

For the rest of paper, we will only work on the dataset that is scaled by  $S^*$ , i.e.,  $\mathbf{X}_{S^*} = S^* \mathbf{X}$ . However, for simplicity, we discard the subscript in later formulations.

## 2.3. Optimization

In this section, we discuss the key detail of the algorithm (Algorithm 1) for solving the optimization problem Eq. (1). In order to handle the binary constraint in Eq. (1), we propose to use alternating optimization over  $\mathbf{V}$  and  $\mathbf{B}$ .

### 2.3.1 Fix $\mathbf{V}$ and update $\mathbf{B}$

When  $\mathbf{V}$  is fixed, the problem becomes exactly the same as when fixing rotation matrix in ITQ [10]. Hence, the optimal value of  $\mathbf{B}$  can be simply achieved by<sup>5</sup>:

$$\mathbf{B} = \text{sign}(\mathbf{XV}). \quad (5)$$

### 2.3.2 Fix $\mathbf{B}$ and update $\mathbf{V}$

When fixing  $\mathbf{B}$ , the optimization is no longer a mix-integer problem. However, the problem is still non-convex and difficult to solve due to the orthonormal constraint. It is important to note that  $\mathbf{V}$  is not a square matrix, i.e., the objective function is not the classic Orthogonal Procrustes problem [24]; hence, we cannot achieve the closed-form solution for  $\mathbf{V}$  as proposed in [10]. To the best of our knowledge, there is no easy way for achieving the closed-form solution

<sup>5</sup>Please refer to ITQ [10] for more detailed explanation.

---

**Algorithm 1** Orthonormal Encoder

---

**Input:**

$\mathbf{X} = \{\mathbf{x}\}_{i=1}^n \in \mathbb{R}^{n \times d}$ : scaled training data;  
 $L$ : code length;  
 $max\_iter$ : maximum iteration number;  
 $\{\epsilon, \epsilon_b, \epsilon_u\}$ : convergence error-tolerances;

**Output**

Column Semi-Orthonormal matrix  $\mathbf{V}$ .

```

1: Initialize  $\mathbf{V} = \mathbf{W}_{PCA}\mathbf{R}$ , where  $\mathbf{W}_{PCA} \in \mathbb{R}^{d \times L}$  and
    $\mathbf{R} \in \mathbb{R}^{L \times L}$  respectively are the PCA dimension reduction
   matrix and ITQ [10] orthogonal rotation matrix.
2: for  $t = 1 \rightarrow max\_iter$  do
3:   procedure FIX  $\mathbf{V}$ , UPDATE  $\mathbf{B}$ .
4:     Compute  $\mathbf{B}$  (Eq. (5)).
5:   procedure FIX  $\mathbf{B}$ , UPDATE  $\mathbf{V}$ .
6:     Find  $\nu_1$  using binary search (BS) (Eq. (9)).
7:     Compute  $\mathbf{v}_1$  (Eq. (8)).
8:     for  $k = 2 \rightarrow L$  do
9:       procedure SOLVE  $\mathbf{v}_k$ 
10:        Initialize  $\Phi_k = [0, \dots, 0]$ .
11:        while true do
12:          Fix  $\Phi_k$ , solve for  $\nu_k$  using BS.
13:          Fix  $\nu_k$ , compute  $\Phi_k = A_k^{-1}c_k$ .
14:          Compute  $\mathbf{v}_k$  (Eq. (13)).
15:          if  $|\mathbf{v}_k^T \mathbf{v}_k - 1| < \epsilon_u$  then
16:            return  $\mathbf{v}_k$ 
17:   if  $t > 1$  and  $|\mathcal{Q}_{t-1} - \mathcal{Q}_t|/\mathcal{Q}_t < \epsilon$  then break
18: return  $\mathbf{V}$ 

```

---

of non-square  $\mathbf{V}$ . Hence, in order to overcome this challenge, inspired by PCA, we use the coordinate descent approach to learn one vector, i.e., one column of  $\mathbf{V}$ , at a time. We now consider two cases for  $k = 1$  and  $2 \leq k \leq L$ .

- **1-st vector**

$$\arg \min_{\mathbf{v}_1} \mathcal{Q}_1 = \frac{1}{n} \|\mathbf{b}_1 - \mathbf{X}\mathbf{v}_1\|^2 \quad \text{s.t. } \mathbf{v}_1^T \mathbf{v}_1 = 1, \quad (6)$$

where  $\|\cdot\|$  is the  $l_2$ -norm.

Let  $\nu_1 \in \mathbb{R}$  be the Lagrange multiplier, we formulate the *Lagrangian*  $\mathcal{L}_1$ :

$$\mathcal{L}_1(\mathbf{v}_1, \nu_1) = \frac{1}{n} \|\mathbf{b}_1 - \mathbf{X}\mathbf{v}_1\|^2 + \nu_1(\mathbf{v}_1^T \mathbf{v}_1 - 1). \quad (7)$$

By minimizing  $\mathcal{L}_1$  over  $\mathbf{v}_1$ , we can achieve:

$$\mathbf{v}_1 = (\mathbf{X}^T \mathbf{X} + n\nu_1 \mathbf{I})^{-1} \mathbf{X}^T \mathbf{b}_1, \quad (8)$$

given  $\nu_1$  that maximizes the *dual function*  $\mathcal{G}_1(\nu_1)$ <sup>6</sup> of  $\mathcal{L}_1(\mathbf{v}_1, \nu_1)$ . Equivalently,  $\nu_1$  should satisfy the following conditions:

---

<sup>6</sup>The dual function  $\mathcal{G}_1(\nu_1)$  can be simply constructed by substituting  $\mathbf{v}_1$  from Eq. (8) into Eq. (7).

$$\begin{cases} \nu_1 > -\lambda_d/n \\ \frac{\partial \mathcal{G}_1}{\partial \nu_1} = [(\mathbf{X}^T \mathbf{X} + n\nu_1 \mathbf{I})^{-1} \mathbf{X}^T \mathbf{b}_1]^T \\ \quad [(\mathbf{X}^T \mathbf{X} + n\nu_1 \mathbf{I})^{-1} \mathbf{X}^T \mathbf{b}_1] - 1 = 0 \end{cases} \quad (9)$$

where  $\lambda_d$  is the smallest eigenvalue of  $\mathbf{X}^T \mathbf{X}$ .

In Eq. (9), the first condition is to make sure that  $(\mathbf{X}^T \mathbf{X} + n\nu_1 \mathbf{I})$  is non-singular and the second condition is achieved by setting the derivative of  $\mathcal{G}_1(\nu_1)$  with regard to  $\nu_1$  equal to 0.

The second equation in Eq. (9) can be recognized as a  $d$ -order polynomial equation of  $\nu_1$  which has no explicit closed-form solution for  $\nu_1$  when  $d > 4$ . Fortunately, since  $\mathcal{G}(\nu_1)$  is a concave function of  $\nu_1$ ,  $\partial \mathcal{G}_1 / \partial \nu_1$  is monotonically decreasing. Hence, we can simply solve for  $\nu_1$  using binary search with a small error-tolerance,  $\epsilon_b$ . Note that:

$$\begin{cases} \lim_{\nu_1 \rightarrow (-\lambda_d/n)^+} \frac{\partial \mathcal{G}_1}{\partial \nu_1} = +\infty \\ \lim_{\nu_1 \rightarrow +\infty} \frac{\partial \mathcal{G}_1}{\partial \nu_1} = -1 \end{cases}, \quad (10)$$

thus  $\partial \mathcal{G}_1 / \partial \nu_1 = 0$  always has a solution.

- **$k$ -th vector** ( $2 \leq k \leq L$ )

For the second vector onward, besides the unit-norm constraint, we also need to make sure that the current vector is independent with its  $(k-1)$  previous vectors.

$$\begin{aligned} \arg \min_{\mathbf{v}_k} \mathcal{Q}_k &= \frac{1}{n} \|\mathbf{b}_k - \mathbf{X}\mathbf{v}_k\|^2 \\ \text{s.t. } \mathbf{v}_k^T \mathbf{v}_k &= 1; \mathbf{v}_k^T \mathbf{v}_i = 0, \forall i \in [1, k-1]. \end{aligned} \quad (11)$$

Let  $\nu_k \in \mathbb{R}$  and  $\Phi_k = [\phi_{k1}, \dots, \phi_{k(k-1)}]^T \in \mathbb{R}^{(k-1)}$  be the Lagrange multipliers, we also formulate the *Lagrangian*  $\mathcal{L}_k$ :

$$\begin{aligned} \mathcal{L}_k(\mathbf{v}_k, \nu_k, \Phi_k) &= \frac{1}{n} \|\mathbf{b}_k - \mathbf{X}\mathbf{v}_k\|^2 \\ &+ \nu_k(\mathbf{v}_k^T \mathbf{v}_k - 1) + \sum_{i=1}^{k-1} \phi_{ki} \mathbf{v}_k^T \mathbf{v}_i. \end{aligned} \quad (12)$$

Minimizing  $\mathcal{L}_k$  over  $\mathbf{v}_k$ , similar to Eq. (8), we can achieve:

$$\mathbf{v}_k = (\mathbf{X}^T \mathbf{X} + n\nu_k \mathbf{I})^{-1} \left( \mathbf{X}^T \mathbf{b}_k - \frac{n}{2} \sum_{i=1}^{k-1} \phi_{ki} \mathbf{v}_i \right), \quad (13)$$

given  $\{\nu_k, \Phi_k\}$  that satisfy the following conditions which make the corresponding *dual function*  $\mathcal{G}_k(\nu_k, \Phi_k)$  maximum:

$$\begin{cases} \nu_k > -\lambda_d/n \\ \mathbf{v}_k^T \mathbf{v}_k = 1 \\ \mathbf{A}_k \Phi_k = \mathbf{c}_k \end{cases} \quad (14)$$

where



$$\begin{cases} \mathbf{A}_k = \frac{n}{2} \begin{bmatrix} \mathbf{v}_1^T \mathbf{Z}_k \mathbf{v}_1 & \cdots & \mathbf{v}_1^T \mathbf{Z}_k \mathbf{v}_{(k-1)} \\ \vdots & \ddots & \vdots \\ \mathbf{v}_{(k-1)}^T \mathbf{Z}_k \mathbf{v}_1 & \cdots & \mathbf{v}_{(k-1)}^T \mathbf{Z}_k \mathbf{v}_{(k-1)} \end{bmatrix} \\ \mathbf{c}_k = \left[ \mathbf{v}_1^T \mathbf{Z}_k \mathbf{X}^T \mathbf{b}_k \quad \cdots \quad \mathbf{v}_{(k-1)}^T \mathbf{Z}_k \mathbf{X}^T \mathbf{b}_k \right]^T \end{cases}$$

in which  $\mathbf{Z}_k = (\mathbf{X}^T \mathbf{X} + n\nu_k \mathbf{I})^{-1}$ .

There is also no straight-forward solution for  $\{\nu_k, \Phi_k\}$ . In order to resolve this issue, we propose to use alternative optimization to solve for  $\nu_k$  and  $\Phi_k$ . In particular, (i) given a fixed  $\Phi_k$  (initialized as  $[0, \dots, 0]^T$ ), we find  $\nu_k$  using binary search as discuss above. Additionally, similar to  $\nu_1$ , there is always a solution for  $\nu_k$ . Then, (ii) with fixed  $\nu_k$ , we can get the closed-form solution for  $\Phi_k$  as  $\Phi_k = \mathbf{A}_k^{-1} \mathbf{c}_k$ . Note that since the dual function  $\mathcal{G}_k$  is a concave function of  $\{\nu_k, \Phi_k\}$ , alternative optimizing between  $\nu_k$  and  $\Phi_k$  still guarantees the solution to approach the global optimal one. We stop this alternative optimization when  $|\mathbf{v}_k^T \mathbf{v}_k - 1| \leq \epsilon_u$ .

Fig. 3 shows an error convergence curve of Eq. (1). We stop the optimization when the relative reduction of the quantization loss is less than  $\epsilon$ , i.e.,  $|\mathcal{Q}_{t-1} - \mathcal{Q}_t|/\mathcal{Q}_t < \epsilon$ .

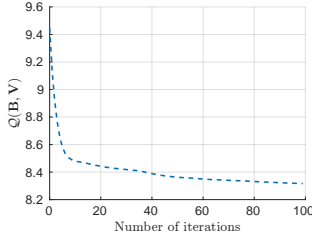


Figure 3: Quantization error for learning the projection matrix  $\mathbf{V}$  with  $L = 32$  on the CIFAR-10 dataset (section 4.1).

### 3. Simultaneous Compression & Quantization: Orthogonal Encoder

#### 3.1. Problem Formulation

In Orthonormal Encoder (OnE), we work with the *column semi-orthonormal* constraint on  $\mathbf{V}$ . However, we recognize that relaxing this constraint to *column semi-orthogonal* constraint, i.e., relaxing the unit norm constraint on each column of  $\mathbf{V}$ , by converting it into a penalty term, provides three important advantages. We now achieve the new loss function as following:

$$\begin{aligned} \arg \min_{\mathbf{B}, \mathbf{V}} \mathcal{Q}(\mathbf{B}, \mathbf{V}) &= \frac{1}{n} \|\mathbf{B} - \mathbf{XV}\|_F^2 + \mu \sum_{i=1}^L \mathbf{v}_i^T \mathbf{v}_i \\ \text{s.t. } \mathbf{B} &\in \{-1, +1\}^{n \times L}; \mathbf{v}_i^T \mathbf{v}_j = 0, \forall i \neq j, \end{aligned} \quad (15)$$

where  $\mu$  is a fixed positive hyper-parameter to penalize large norms of  $\mathbf{v}_i$ .

Firstly, with an appropriately large  $\mu$ , the optimization prefers to choose large variance components of  $\mathbf{X}$  since this helps to achieve the projection vectors that have smaller

norms. In other words, without penalizing large norms of  $\mathbf{v}_i$ , the optimization has no incentive to focus on high variance components of  $\mathbf{X}$  since it can produce projection vectors with arbitrary large norms that can scale any components appropriately to achieve minimum binary quantization loss. Secondly, this provides more flexibility of having different scale values for different directions. Consequently, relaxing the unit-norm constraint of each column of  $\mathbf{V}$  helps to mitigate the difficulty of choosing the scale value  $\mathcal{S}$ . However, on the other hand, a too large  $\mu$  may distract the optimization from minimizing the binary quantization term. Finally, from OnE Optimization (Section 2.3), we observed that the unit norm constraint on each column of  $\mathbf{V}$  makes the OnE optimization difficult to be solved efficiently since there is no closed-form solution for  $\{\mathbf{v}\}_{k=1}^L$ . By relaxing this unit norm constraint, we now can achieve the closed-form solutions for  $\{\mathbf{v}\}_{k=1}^L$ ; hence, it is very computationally beneficial.

#### 3.2. Optimization

Similar to the Algorithm 1 for solving Orthonormal Encoder, we apply alternative optimize  $\mathbf{V}$  and  $\mathbf{B}$  with the  $\mathbf{B}$  step is exactly the same as Eq. (5). For  $\mathbf{V}$  step, we also utilize the coordinate descent approach to iteratively solve  $\mathbf{V}$ , i.e., column by column. The loss functions are rewritten and their corresponding closed-form solutions for  $\{\mathbf{v}\}_{k=1}^L$  can be efficiently achieved as following:

- 1-st vector

$$\arg \min_{\mathbf{v}_1} \mathcal{Q}_1 = \frac{1}{n} \|\mathbf{b}_1 - \mathbf{Xv}_1\|^2 + \mu \mathbf{v}_1^T \mathbf{v}_1. \quad (16)$$

We can see that Eq. (16) is the regularized least squares problem, whose closed-form solution is given as:

$$\mathbf{v}_1 = (\mathbf{X}^T \mathbf{X} + n\mu \mathbf{I})^{-1} \mathbf{X}^T \mathbf{b}_1. \quad (17)$$

- $k$ -th vector ( $2 \leq k \leq L$ )

$$\begin{aligned} \arg \min_{\mathbf{v}_k} \mathcal{Q}_k &= \frac{1}{n} \|\mathbf{b}_k - \mathbf{Xv}_k\|^2 + \mu \mathbf{v}_k^T \mathbf{v}_k \\ \text{s.t. } \mathbf{v}_k^T \mathbf{v}_i &= 0, \forall i \in [1, k-1]. \end{aligned} \quad (18)$$

Given the Lagrange multiplier  $\Phi_k = [\phi_{k1}, \dots, \phi_{k(k-1)}]^T \in \mathbb{R}^{(k-1)}$ , similar to Eq. (8) and Eq. (12), we can obtain  $\mathbf{v}_k$  as following:

$$\mathbf{v}_k = (\mathbf{X}^T \mathbf{X} + n\mu \mathbf{I})^{-1} \left( \mathbf{X}^T \mathbf{b}_k - \frac{n}{2} \sum_{i=1}^{k-1} \phi_{ki} \mathbf{v}_i \right), \quad (19)$$

where  $\Phi_k = \mathbf{A}_k^{-1} \mathbf{c}_k$ , in which

$$\begin{cases} \mathbf{A}_k = \frac{n}{2} \begin{bmatrix} \mathbf{v}_1^T \mathbf{Zv}_1 & \cdots & \mathbf{v}_1^T \mathbf{Zv}_{(k-1)} \\ \vdots & \ddots & \vdots \\ \mathbf{v}_{(k-1)}^T \mathbf{Zv}_1 & \cdots & \mathbf{v}_{(k-1)}^T \mathbf{Zv}_{(k-1)} \end{bmatrix} \\ \mathbf{c}_k = \left[ \mathbf{v}_1^T \mathbf{Z}\mathbf{X}^T \mathbf{b}_k \quad \cdots \quad \mathbf{v}_{(k-1)}^T \mathbf{Z}\mathbf{X}^T \mathbf{b}_k \right]^T \end{cases}$$

and  $\mathbf{Z} = (\mathbf{X}^T \mathbf{X} + n\mu \mathbf{I})^{-1}$ . Additionally, given a fixed  $\mu$ ,  $\mathbf{Z}$  is a constant, the  $(k-1) \times (k-1)$  matrix  $\mathbf{A}_k$  contains  $(k-2) \times (k-2)$  matrix  $\mathbf{A}_{(k-1)}$  in the top-left corner. It means that only the  $(k-1)$ -th row and column of matrix  $\mathbf{A}_k$  are needed to be computed. Thus,  $\Phi_k$  can be solved even more effectively.

Similar to OnE (Fig. 3), we also empirically observe the convergence of the optimization problem Eq. 15. We summarize the Orthogonal Encoder method in Algorithm 2.

---

**Algorithm 2** Orthogonal Encoder

---

**Input:**

$\mathbf{X} = \{\mathbf{x}\}_{i=1}^n \in \mathbb{R}^{n \times d}$ : scaled training data;  
 $L$ : code length;  
 $max\_iter$ : maximum iteration number;  
 $\epsilon$ : convergence error-tolerance;

**Output**

Column Semi-Orthogonal matrix  $\mathbf{V}$ .

- 1: Initialize  $\mathbf{V} = \mathbf{W}_{PCA} \mathbf{R}$ , where  $\mathbf{W}_{PCA} \in \mathbb{R}^{d \times L}$  and  $\mathbf{R} \in \mathbb{R}^{L \times L}$  respectively are the PCA dimension reduction matrix and ITQ [10] orthogonal rotation matrix.
  - 2: **for**  $t = 1 \rightarrow max\_iter$  **do**
  - 3:   Fix  $\mathbf{V}$ , update  $\mathbf{B}$ : Compute  $\mathbf{B}$  (Eq. (5)).
  - 4:   Fix  $\mathbf{B}$ , update  $\mathbf{V}$ : Compute  $\{\mathbf{v}_i\}_{i=1}^L$  (Eq.(17),(19)).
  - 5:   **if**  $t > 1$  and  $|\mathcal{Q}_{t-1} - \mathcal{Q}_t|/\mathcal{Q}_t < \epsilon$  **then break**
  - 6: **return**  $\mathbf{V}$
- 

## 4. Experiments

### 4.1. Datasets, Evaluation protocols, and Implementation notes

The **CIFAR-10 dataset** [15] contains 60,000 fully-annotated color images of  $32 \times 32$  from 10 object classes (6,000 images for each class). The provided test set (1,000 images for each class) is used as the query set. The remaining 50,000 images are used as training set and database.

The **LabelMe-12-50k dataset** [27] consists of 50,000 fully-annotated color images of  $256 \times 256$  of 12 object classes, which is a subset of LabelMe dataset [23]. In this dataset, for images having multiple label values in  $[0.0, 1.0]$ , the object class of the largest label value is chosen as image label. We also use the provided test set as query set and the remaining images as training set and database.

The **SUN397 dataset** [34] contains about 108,000 fully-annotated color images from 397 scene categories. We select a subset of 42 categories which contain more than 500 images (about 35,000 images in total). We then randomly sample 100 images per class to form the query set. The remaining images are used as training set and database.

For all datasets, each image is represented by a 4096-D feature vector extracted from the fully-connected layer 7 of pre-trained VGG [26].

**Evaluation protocols.** We apply three standard evaluation metrics, which are widely used in literature [2, 8, 10], to measure the retrieval performance of all methods: 1) mean Average Precision (**mAP**(%)); 2) precision at Hamming radius of 2 (**prec@r2** (%)) which measures precision on retrieved images having Hamming distance to query  $\leq 2$  (we report zero precision for the queries that return no image); 3) precision at top 1000 return images (**prec@1k** (%)) which measures the precision on the top 1000 retrieved images. Class labels are used as ground truths for all evaluation. Additionally, to avoid biased results due to unbalanced samples of different classes in the query sets, we calculate the average results for all classes.

**Implementation notes.** For computational efficiency, we apply PCA to reduce the feature dimension to 512-D. For OgE method, the hyper-parameter is empirically set as:  $\mu = 0.02$ . The maximum number of iteration is set as 100. Finally, we set all error-tolerance values,  $\epsilon$ ,  $\epsilon_b$ ,  $\epsilon_n$ , as  $10^{-4}$ .

For all compared methods: Spherical Hashing (SpH) [13], K-means Hashing (KMH)<sup>7</sup> [12], Binary Autoencoder (BA) [2], and Iterative Quantization (ITQ) [10]; we use the implementation with suggested parameters provided by the authors. Besides, to improve the statistical stability in the results, we report the average values of 5 executions.

### 4.2. Comparison with state-of-the-art

In this section, we evaluate our proposed hashing methods, SCQ - OnE and OgE, and compare to the state-of-the-art unsupervised hashing methods including SpH, KMH, BA, and ITQ. The experimental results in **mAP**, **prec@r2** and **prec@1k** are reported in Table 1. Our proposed methods clearly achieves significant improvement over all datasets at the majority of evaluation metrics. The improvement gaps are clearer at higher code lengths, i.e.,  $L = 32$ . Additionally, OgE generally achieves slightly higher performance than OnE. Moreover, it is noticeable that, for **prec@r2**, all compared methods suffer performance downgrade at long hash code, e.g.,  $L = 32$ . However, our proposed methods still achieve good **prec@r2** at  $L = 32$ . This shows that binary codes producing by our methods highly preserve data similarity.

**Comparison with Deep Hasing (DH) [8] and Unsupervised Hashing with Binary Deep Neural Network (UH-BDNN) [4].** Recently, there are several methods [8, 4] applying DNN to learn binary hash code, which achieved very competitive performances. Hence, in order to have a complete evaluation, following the experiment settings of [8, 4], we conduct experiments on CIFAR-10 dataset. In this experiment, 100 images are randomly sampled for each class as a query set; the remaining images are for training and database. Each image is presented by a GIST 512-D

<sup>7</sup>Due to very long training time at high-dimension of KMH [12], we apply PCA to reduce dimension from 4096-D to 512-D.

Table 1: Performance comparison with the state-of-the-art unsupervised hashing methods.

The **Bold** and Underline values indicate the **best** and second best performances respectively.

	Dataset	CIFAR-10 [15]				LabelMe-12-50k [27]				SUN397 [34]			
	L	8	16	24	32	8	16	24	32	8	16	24	32
<i>mAP</i>	SpH [13]	17.09	18.77	20.19	20.96	11.68	13.24	14.39	14.97	9.13	13.53	16.63	19.07
	KMH [12]	14.26	15.55	24.20	23.12	14.70	12.79	16.99	15.09	21.91	23.42	26.04	29.17
	BA [2]	23.24	24.02	24.77	25.92	17.48	17.10	17.91	18.07	20.73	31.18	35.36	36.40
	ITQ [10]	24.75	26.47	26.86	27.19	17.56	17.73	18.52	19.09	20.16	30.95	35.92	37.84
	SCQ - OnE	<u>27.08</u>	<b>29.64</b>	<u>30.57</u>	<u>30.82</u>	19.76	<u>21.96</u>	<b>23.61</b>	<u>24.25</u>	<u>23.37</u>	<u>34.09</u>	<u>38.13</u>	<u>40.54</u>
	SCQ - OgE	<b>26.98</b>	29.33	<b>30.65</b>	<b>31.15</b>	<b>20.63</b>	<b>23.07</b>	<u>23.54</u>	<b>24.68</b>	<b>23.44</b>	<b>34.73</b>	<b>39.47</b>	<b>41.82</b>
<i>prec@r2</i>	SpH	18.04	30.58	37.28	21.40	11.72	19.38	25.14	13.66	6.88	23.68	37.21	27.39
	KMH	12.42	34.01	42.33	27.46	9.93	26.17	32.09	18.62	9.50	<u>36.14</u>	<b>51.27</b>	39.29
	BA	23.67	38.05	42.95	23.49	16.22	25.75	31.35	13.14	<b>10.50</b>	<b>37.75</b>	<u>50.38</u>	41.11
	ITQ	<u>24.38</u>	<b>38.41</b>	<u>42.96</u>	28.63	15.86	25.46	31.43	17.66	<u>9.78</u>	35.15	49.85	46.34
	SCQ - OnE	<b>24.48</b>	36.49	41.53	<u>43.90</u>	<b>16.69</b>	<u>27.30</u>	<u>34.63</u>	<u>33.04</u>	8.68	30.12	43.54	<u>50.41</u>
	SCQ - OgE	24.35	38.30	<b>43.01</b>	<b>44.01</b>	<u>16.57</u>	<b>27.80</b>	<b>34.77</b>	<b>34.64</b>	8.76	29.31	45.03	<b>51.88</b>
<i>prec@1k</i>	SpH	22.93	26.99	29.50	31.98	14.07	16.78	18.52	19.27	10.79	15.36	18.21	20.07
	KMH	26.64	25.83	34.52	30.75	16.33	14.97	21.41	19.02	18.94	22.93	23.74	27.26
	BA	31.73	34.16	35.67	37.01	21.14	21.71	22.64	22.83	19.22	28.68	31.31	31.80
	ITQ	32.40	36.35	37.25	37.96	21.01	22.00	22.98	23.63	18.86	28.62	31.56	32.74
	SCQ - OnE	<u>33.38</u>	<u>37.82</u>	<u>39.13</u>	<u>40.40</u>	<u>22.91</u>	<u>25.39</u>	<u>26.55</u>	<u>27.16</u>	<u>19.26</u>	<u>29.95</u>	<u>32.72</u>	<u>34.08</u>
	SCQ - OgE	<b>33.41</b>	<b>38.33</b>	<b>39.54</b>	<b>40.70</b>	<b>23.94</b>	<b>25.94</b>	<b>26.99</b>	<b>27.46</b>	<b>20.10</b>	<b>29.95</b>	<b>33.43</b>	<b>35.00</b>

descriptor [21]. In addition, to avoid bias results due to test samples, we repeat the experiment 5 times with 5 different random training/query sets. The comparative results in term of *mAP* and *prec@r2* are presented in Table 2. Our proposed methods are very competitive with DH and UH-BDNN, specifically achieving higher *mAP* and *prec@r2* at  $L = 32$  than DH and UH-BDNN.

Table 2: Performance comparison in *mAP* with Deep Hashing (DH) and Unsupervised Hashing with Binary Deep Neural Network (UH-BDNN) on CIFAR-10 dataset. The **Bold** values indicate the **best** performances.

	Methods	<i>mAP</i>		<i>prec@r2</i>	
		16	32	16	32
CIFAR-10	DH [8]	16.17	16.62	23.33	15.77
	UH-BDNN [4]	17.83	18.52	<b>24.97</b>	18.85
	SCQ - OnE	17.97	18.63	24.57	23.72
	SCQ - OgE	<b>18.00</b>	<b>18.78</b>	24.15	<b>25.69</b>

### 4.3. Training time and Processing time

In this experiment, we empirically evaluate the training time and online processing time of our methods. The experiments are carried out on a workstation with a 4-core i7-6700 CPU @ 3.40GHz. The experiments are conducted on the combination of CIFAR-10, Labelme-12-50k, and SUN397 datasets. For OnE and OgE, the training time include time for applying zero-mean, scaling, reducing dimension to  $D = 512$  and ITQ initialization (50 iterations). We use 50 iterations for all experiments. The Fig. 4 shows that our proposed methods, OnE and OgE, are very efficient. OgE is just slightly slower than ITQ [10]. Even though OnE is much slower than OgE and ITQ, it takes just over a

minute for 100,000 training samples which is still very fast and practical, in comparison with several dozen minutes (up to hours) for BA [2] and UH-BDNN [4]<sup>8</sup>.

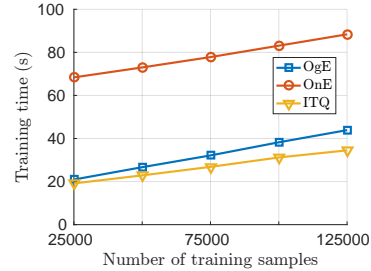


Figure 4: The training time for learning 32-bit hash code embedding.

Compared with training cost, the time to produce new hash codes is more important since it is done in real time. Similar to Semi-Supervised Hashing (SSH) [28] and ITQ [10], by using only a single linear transformation, our proposed methods require only one BLAS operation (`gemv` or `gemm`) and a comparison operation; hence, it takes negligible time to produce binary codes for new data points.

## 5. Conclusion

In this paper, we successfully addressed the problem of jointly learning to preserve data pairwise (dis)similarity in low-dimension space and minimize the binary quantization loss. Extensive experiments on various datasets show that both our proposed methods, Simultaneous Compression

<sup>8</sup>For training 50000 CIFAR-10 samples using author's release code and dataset [4].



and Quantization (SCQ): Orthonormal Encoder (OnE) and Orthogonal Encoder (OgE), outperform other state-of-the-art hashing methods by a clear margin under the three standard evaluation metrics. Moreover, OgE achieves slightly higher performance while having much shorter training times than OnE.

## References

- [1] A. Andoni and P. Indyk. Near-optimal hashing algorithms for approximate nearest neighbor in high dimensions. *Commun. ACM*, 51, Jan. 2008. 1, 2
- [2] M. Á. Carreira-Perpiñán and R. Raziperchikolaei. Hashing with binary autoencoders. In *CVPR*, 2015. 1, 7, 8
- [3] T.-T. Do and N.-M. Cheung. Embedding based on function approximation for large scale image search. *TPAMI*, 2017. 1
- [4] T.-T. Do, A.-D. Doan, and N.-M. Cheung. Learning to hash with binary deep neural network. In *ECCV*, 2016. 1, 2, 7, 8
- [5] T.-T. Do, A.-D. Doan, D.-T. Nguyen, and N.-M. Cheung. Binary hashing with semidefinite relaxation and augmented lagrangian. In *ECCV*, 2016. 1
- [6] T.-T. Do, D.-K. Le Tan, T. T. Pham, and N.-M. Cheung. Simultaneous feature aggregating and hashing for large-scale image search. In *CVPR*, 2017. 1
- [7] T.-T. Do, Q. Tran, and N.-M. Cheung. FAemb: A function approximation-based embedding method for image retrieval. In *CVPR*, 2015. 1
- [8] V. Erin Liong, J. Lu, G. Wang, P. Moulin, and J. Zhou. Deep hashing for compact binary codes learning. In *CVPR*, 2015. 7, 8
- [9] A. Gionis, P. Indyk, and R. Motwani. Similarity search in high dimensions via hashing. In *VLDB*, 1999. 1
- [10] Y. Gong and S. Lazebnik. Iterative quantization: A procrustean approach to learning binary codes. In *CVPR*, 2011. 1, 2, 3, 4, 5, 7, 8
- [11] K. Grauman and R. Fergus. Learning binary hash codes for large-scale image search. 411, 01 2013. 1
- [12] K. He, F. Wen, and J. Sun. K-means hashing: An affinity-preserving quantization method for learning binary compact codes. In *CVPR*, 2013. 1, 7, 8
- [13] J. P. Heo, Y. Lee, J. He, S. F. Chang, and S. E. Yoon. Spherical hashing. In *CVPR*, 2012. 1, 7, 8
- [14] T. Hoang, T.-T. Do, D.-K. L. Tan, and N.-M. Cheung. Selective deep convolutional features for image retrieval. In *ACM-MM*, 2017. 1
- [15] A. Krizhevsky and G. Hinton. Learning multiple layers of features from tiny images. In *Technical report, University of Toronto*, 2009. 7, 8
- [16] B. Kulis and T. Darrell. Learning to hash with binary reconstructive embeddings. In Y. Bengio, D. Schuurmans, J. D. Lafferty, C. K. I. Williams, and A. Culotta, editors, *NIPS*, 2009. 1
- [17] B. Kulis and K. Grauman. Kernelized locality-sensitive hashing for scalable image search. In *ICCV*, Nov 2009. 1
- [18] G. Lin, C. Shen, Q. Shi, A. van den Hengel, and D. Suter. Fast supervised hashing with decision trees for high-dimensional data. In *CVPR*, 2014. 1
- [19] W. Liu, J. Wang, R. Ji, Y. G. Jiang, and S. F. Chang. Supervised hashing with kernels. In *CVPR*, 2012. 1
- [20] M. Norouzi, D. J. Fleet, and R. Salakhutdinov. Hamming distance metric learning. In *NIPS*, 2012. 1
- [21] A. Oliva and A. Torralba. Modeling the shape of the scene: A holistic representation of the spatial envelope. *IJCV*, pages 145–175, 2001. 8
- [22] M. Raginsky and S. Lazebnik. Locality-sensitive binary codes from shift-invariant kernels. In Y. Bengio, D. Schuurmans, J. D. Lafferty, C. K. I. Williams, and A. Culotta, editors, *NIPS*. 2009. 1
- [23] B. C. Russell, A. Torralba, K. P. Murphy, and W. T. Freeman. Labelme: A database and web-based tool for image annotation. *IJCV*, pages 157–173, 2008. 7
- [24] P. H. Schönemann. A generalized solution of the orthogonal procrustes problem. *Psychometrika*, 1966. 4
- [25] F. Shen, C. Shen, W. Liu, and H. T. Shen. Supervised discrete hashing. In *CVPR*, 2015. 1
- [26] K. Simonyan and A. Zisserman. Very deep convolutional networks for large-scale image recognition. *CoRR*, 2014. 7
- [27] R. Uetz and S. Behnke. Large-scale object recognition with cuda-accelerated hierarchical neural networks. In *IEEE International Conference on Intelligent Computing and Intelligent Systems (ICIS)*, 2009. 7, 8
- [28] J. Wang, S. Kumar, and S. F. Chang. Semi-supervised hashing for large-scale search. *TPAMI*, 2012. 2, 8
- [29] J. Wang, W. Liu, S. Kumar, and S. Chang. Learning to hash for indexing big data - a survey. 104, 09 2015. 1
- [30] J. Wang, H. Tao Shen, J. Song, and J. Ji. Hashing for similarity search: A survey. 08 2014. 1
- [31] J. Wang, T. Zhang, j. song, N. Sebe, and H. T. Shen. A survey on learning to hash. *TPAMI*, 2017. 1
- [32] Y. Weiss, A. Torralba, and R. Fergus. Spectral hashing. In *NIPS*, 2009. 1, 2
- [33] Z. Wen and W. Yin. A feasible method for optimization with orthogonality constraints. *Math. Program.*, Dec 2013. 2
- [34] J. Xiao, K. A. Ehinger, J. Hays, A. Torralba, and A. Oliva. Sun database: Exploring a large collection of scene categories. *IJCV*, Aug 2016. 7, 8
- [35] D. Zhang, J. Wang, D. Cai, and J. Lu. Self-taught hashing for fast similarity search. In *ACM SIGIR*, 2010. 1